International Journal of Pressure Vessels and Piping 87 (2010) 396–401

Contents lists available at ScienceDirect

International Journal of Pressure Vessels and Piping

journal homepage: www.elsevier.com/locate/ijpvp

Residual stress analysis of autofrettaged thick-walled spherical pressure vessel

M. Maleki [a,*], G.H. Farrahi [a], B. Haghpanah Jahromi [a,b], E. Hosseinian [a]

[a] School of Mechanical Engineering, Sharif University of Technology, Tehran, Iran
[b] Department of Mechanical and Industrial Engineering, Northeastern University, Boston, USA

ARTICLE INFO

Article history:
Received 20 January 2010
Received in revised form
13 April 2010
Accepted 26 April 2010

Keywords:
Autofrettage
Spherical pressure vessel
Residual stress
Extended variable material properties method
Optimum autofrettage pressure

ABSTRACT

In this study, residual stress distributions in autofrettaged homogenous spherical pressure vessels subjected to different autofrettage pressures are evaluated. Results are obtained by developing an extension of variable material properties (VMP) method. The modification makes VMP method applicable for analyses of spherical vessels based on actual material behavior both in loading and unloading and considering variable Bauschinger effect. The residual stresses determined by employing finite element method are compared with VMP results and it is demonstrated that the using of simplified material models can cause significant error in estimation of hoop residual stress, especially near the inner surface of the vessel. By performing a parametric study, the optimum autofrettage pressure and corresponding autofrettage percent for creating desirable residual stress state are introduced and determined.

1. Introduction

Hydraulic autofrettage is a process in which a cylindrical or spherical pressure vessel is subjected to high internal pressure till its wall becomes partially plastic. The resulting compressive hoop residual stress produced after removing the pre-pressure improves the fatigue life and load capability of the vessel [1–3]. This specification besides a comparatively reasonable cost of the process has caused frequent and vast use of autofrettaged vessels in a variety of applications, especially in the case of high and cyclic applied internal pressure.

Spherical pressure vessels, despite difficulties in manufacturing, due to appropriate stress and strain distributions are extensively used in critical applications. Although, the study of autofrettage technique in tubes has been the subject of several research projects [4–7], autofrettage of spherical pressure vessels was only recently considered [8–13]. Adibi-asl and Livieri [8] proposed an analytical method for residual stress analyses of autofrettaged spherical vessels. Their investigation is limited to materials which follow a constrained form of modified Ramberg-Osgood, Isotropic or kinematic hardening models during loading and unloading. Kargarnovin et al. [10] applied an elastic-linear work hardening model and ignored the Bauschinger effect to evaluate optimum prestressing pressure in a spherical vessel. While the response of the material models applied in these investigations are not compatible with the actual behavior of several of the most used materials in pressure vessels [14,15], their results can not be reliably employed. Parker and Huang [12] put forward analytical solution of autofrettaged spherical vessels incorporating more sensible material model and verified their established method by comparing the results of developed variable material property method at particular autofrettage percents. Perl and Perry [13] extended the existing knowledge to provide more realistic solutions for the residual stress fields in thick-walled autofrettaged spherical pressure vessels. Applying the minimum weight and the maximum life criterion, they also proposed an optimum design of autofrettage process.

It is thanks to previous research efforts that a proper approximation of residual stress distribution in spherical pressure vessels is achievable now, but still need to be more investigated.

To analyze the residual stress distribution induced by autofrettage process of a thick-walled spherical pressure vessel, we employ an extension of the variable material property (VMP) method introduced by Jahed and Dubey [16] and compared the obtained results with the results of finite element analyses. In the VMP method, the linear elastic solution of a boundary value problem is used as a basis to generate its inelastic solution. The material parameters are considered as field variables and their distribution is obtained as a part of solution in an iterative manner. This method was generally employed to homogeneous and inhomogeneous cylindrical pressure vessel and rotating disks [17–21]. The proposed extension makes the VMP method capable for

* Corresponding author. Tel.: +41 21 693 29 74; fax: +41 21 693 73 40.
E-mail address: milad.maleki@epfl.ch (M. Maleki).

0308-0161/$ – see front matter © 2010 Elsevier Ltd. All rights reserved.
doi:10.1016/j.ijpvp.2010.04.002

analyzing the residual stresses in autofrettaged spherical pressure vessels. The main advantage of this method is its capability in the implementation of actual behavior of material obtained from loading and unloading tests in the analyses.

In addition, the optimum pressure for autofrettage of the spherical pressure vessels made of A723 and HB7 steels is discussed here. In this study, an autofrettage percent has been defined as the optimum value by which the significant compressive hoop residual stress at inner surface of the vessel is achievable, while simultaneously the tensional hoop residual stress at outer surface is relatively low.

2. Theoretical model

The components of total strain of an infinitesimally small element located at a distance r from the center of a thick-walled sphere can be represented as summation of elastic, ε_{ij}^{e} and plastic, ε_{ij}^{p}, strain components. The elastic part is given as,

$$\varepsilon_{ij}^{e} = \left(\frac{1+\nu}{E}\right)\sigma_{ij} - \left(\frac{\nu}{E}\right)\sigma_{kk}\delta_{ij} \tag{1}$$

where δ_{ij}, E, ν are the Kronecker delta, elastic modulus and Poisson's ratio respectively. The plastic part of strain is given by Hencky's total deformation equation, $\varepsilon_{ij}^{p} = \phi(\sigma_{ij} - \frac{1}{3}\sigma_{kk}\delta_{ij})$ where ϕ is a scalar function given by $\phi = \frac{3}{2}\frac{\varepsilon_{eq}^{p}}{\sigma_{eq}}$, where ε_{eq}^{p} and σ_{eq} are the equivalent plastic strain and equivalent stress, respectively. Consequently the total strain in the element can be written as,

$$\varepsilon_{ij} = \left(\frac{1+\nu}{E} + \phi\right)\sigma_{ij} - \left(\frac{\nu}{E} + \frac{1}{3}\phi\right)\sigma_{kk}\delta_{ij} \tag{2}$$

In order to analyze a thick-walled spherical vessel, we divide the vessel into a number of concentric thin spheres (layers) through the thickness, where the inner radius of the interior layer and the outer radius of exterior layer are equal to interior and exterior radii of the vessel.

According to VMP approach, the total strain components of each elasto-plastic layer can be calculated by the following equation:

$$\varepsilon_{ij} = \frac{1+\nu_{eq}(r)}{E_{eq}(r)}\sigma_{ij} - \frac{\nu_{eq}(r)}{E_{eq}(r)}\sigma_{kk}\delta_{ij} \tag{3}$$

where $\nu_{eq}(r)$ and $E_{eq}(r)$ are equivalent Poisson's ratio and equivalent elastic modulus of a layer with distance of r from the center of sphere. Comparing equations (2) and (3), the following relationships are obtained:

$$E_{eq}(r) = \frac{3E}{3+2E\phi} \tag{4}$$

$$\nu_{eq}(r) = \frac{E_{eq}(r)(2\nu-1)+E}{2E} \tag{5}$$

Based on the VMP method, the elasto-plastic solution is achievable by implementation of appropriate variable material constants and performing the equivalent elastic analysis.

The elastic solution of a spherical layer with inner and outer radii of r_i and r_{i+1} and material constants of ν_{eq} and E_{eq} is:

$$u = \frac{(p_i r_i^3 - p_{i+1}r_{i+1}^3)(1+\nu_{eq})(1-2\nu_{eq})}{E_{eq}(1-\nu_{eq})\left(r_{i+1}^3 - r_i^3\right)}r + \frac{r_i^3 r_{i+1}^3(p_i - p_{i+1})(1+\nu_{eq})}{2E_{eq}\left(r_{i+1}^3 - r_i^3\right)r^2} \tag{6}$$

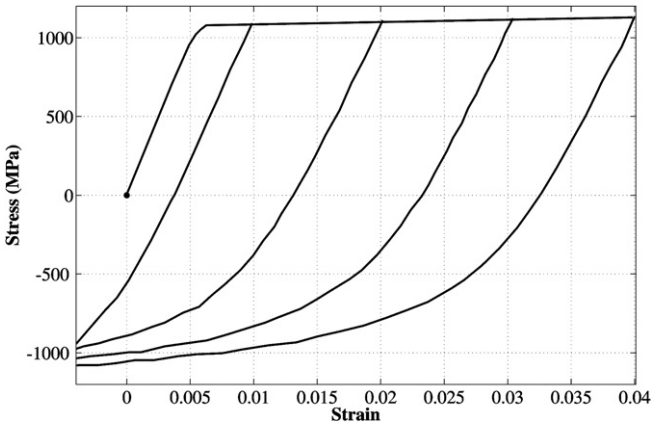

Fig. 1. Engineering stress-strain curve of A723 steel, after Toriano et al. [23].

$$\sigma_{rad} = \frac{p_i r_i^3 - p_{i+1}r_{i+1}^3}{r_{i+1}^3 - r_i^3} - \frac{r_i^3 r_{i+1}^3(p_i - p_{i+1})}{r^3\left(r_{i+1}^3 - r_i^3\right)}$$

$$\sigma_{\theta} = \sigma_{\phi} = \frac{p_i r_i^3 - p_{i+1}r_{i+1}^3}{r_{i+1}^3 - r_i^3} + \frac{r_i^3 r_{i+1}^3(p_i - p_{i+1})}{2r^3\left(r_{i+1}^3 - r_i^3\right)} \tag{7}$$

where p_i and p_{i+1} are internal and external pressures, u is radial displacement and σ_{rad}, σ_{θ} and σ_{ϕ} are stress components.

Based on equation (6), the inside and outside displacements of each layer located at r, u_i and u_{i+1}, are related to the inside and outside pressures by:

$$\begin{bmatrix} c_{11,r} & c_{12,r} \\ c_{21,r} & c_{22,r} \end{bmatrix}^{-1} \begin{bmatrix} u_i \\ u_{i+1} \end{bmatrix} = \begin{bmatrix} p_i \\ p_{i+1} \end{bmatrix} \tag{8}$$

where:

$$c_{11,r} = \frac{r_i\left[(1-2\nu_{eq}(r))r_i^3 + r_{i+1}^3\right]}{E_{eq}(r)\left(r_{i+1}^3 - r_i^3\right)}$$

$$c_{21,r} = \frac{2r_{i+1}r_i^3(1-\nu_{eq}(r))}{E_{eq}(r)\left(r_{i+1}^3 - r_i^3\right)}$$

$$c_{12,r} = \frac{2r_i r_{i+1}^3(\upsilon_{eq}(r)-1)}{E_{eq}(r)\left(r_{i+1}^3 - r_i^3\right)}$$

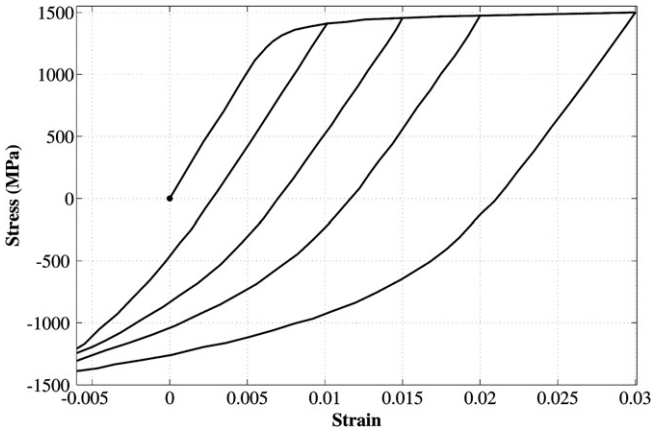

Fig. 2. Engineering stress-strain curve of HB7 steel, after Troiano et al. [22].

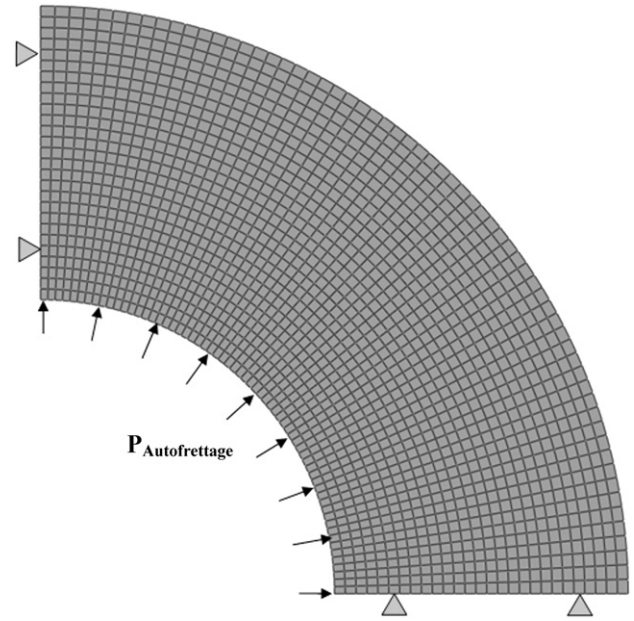

Fig. 3. Finite element model used in residual stress analysis.

$$c_{22,r} = \frac{r_{i+1}\left[(2\nu_{eq}(r)-1)r_{i+1}^3 - r_i^3\right]}{E_{eq}(r)\left(r_{i+1}^3 - r_i^3\right)} \tag{9}$$

After assembling all layers together, a system of linear equations in the form of $[C'][U] = [P]$ is obtained and solved for $[U]$. Then, by calculating p_i and p_{i+1} from equation (8), stresses can be obtained from equation (7).

To evaluate the state of stress in the thick-walled spherical pressure vessel, first, we assume $E_{eq}(r) = E$ and $\nu_{eq}(r) = \nu$ for all layers. Once the state of stress in the vessel is obtained, $E_{eq}(r)$ is updated for each layer based on the calculated equivalent stress by using the projection method [16]. Then, the equivalent Poisson's ratio for each layer, $\nu_{eq}(r)$, is obtained using equation (5). In the next step, the state of stress in each layer is re-calculated from equations (6)–(9) using the updated values of equivalent elastic modulus and equivalent Poisson's ratio. This procedure is continued until the convergence to the stress solution is achieved. This method gives the elasto-plastic stresses in the spherical vessel during loading. Residual stress analysis requires also finding the unloading solution. The unloading solution is similar to loading. While each layer follows its own nonlinear unloading behavior which depends on the equivalent stress of layer induced in loading. Finally, residual stress state is determined by subtracting loading and unloading stresses of each layer.

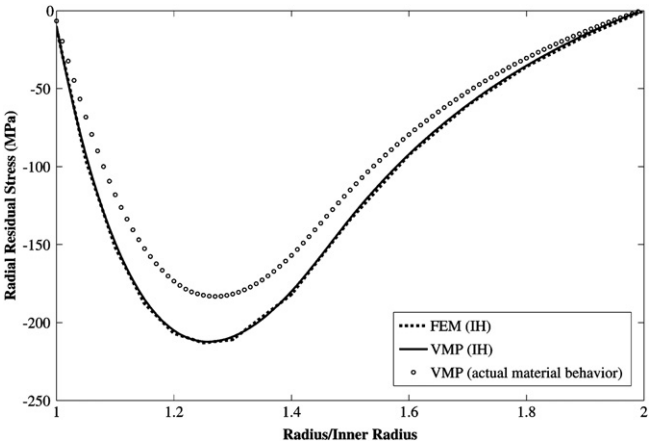

Fig. 5. Radial residual stress distribution of A723 spherical vessel subjected to 1300 MPa autofrettage pressure.

3. Materials

In the manufacture of pressure vessels, improved high strength steels such as A723 and HB7, because of their enhanced toughness and fatigue property, have been proposed and frequently used in critical applications. A723 and HB7 are Cr-Mo-V steels which are produced to an extremely high purity level. HB7 contains lower levels of sulfur, phosphorus and silicon, but in return higher contents of carbon, nickel and carbide formers like chromium, molybdenum and vanadium when compared to A723 steel. Increased level of nickel content and fine grain size of HB7 steel cause a superior fracture toughness. More descriptions on chemical composition and mechanical properties of A723 and HB7 steels can be found in [22]. Because of global interest in these two types of materials, they were selected for residual stress analyses in this study.

The results of series of uniaxial tension-compression tests on A723 and HB7 steels were given by Troiano et al. [22,23] and reproduced here in Figs. 1 and 2 respectively. These steels have approximately elastic-perfectly plastic behavior in loading.

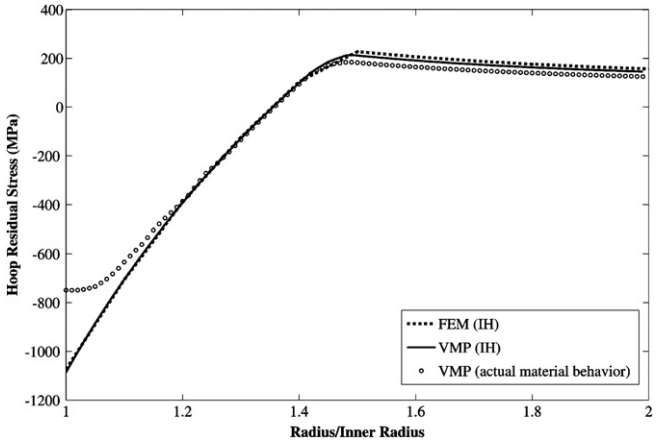

Fig. 4. Hoop residual stress distribution of A723 spherical vessel subjected to 1300 MPa autofrettage pressure.

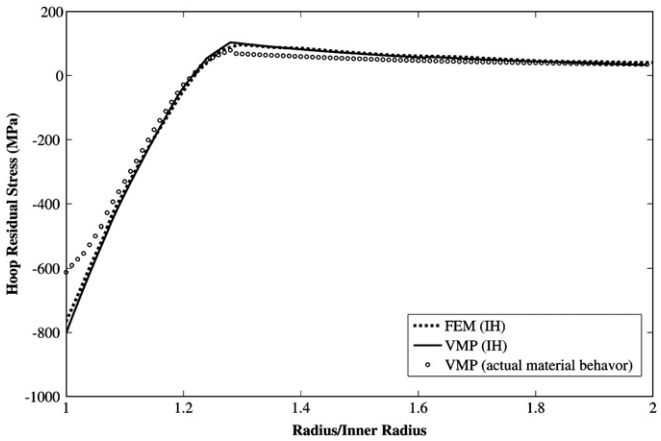

Fig. 6. Hoop residual stress distribution of HB7 spherical vessel subjected to 1330 MPa autofrettage pressure.

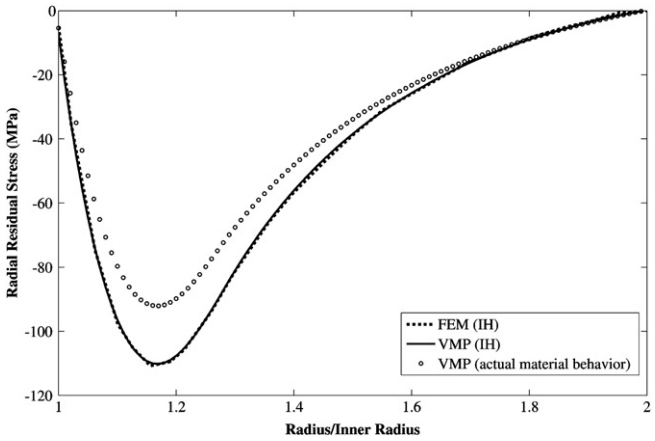

Fig. 7. Radial residual stress distribution of HB7 spherical vessel subjected to 1330 MPa autofrettage pressure.

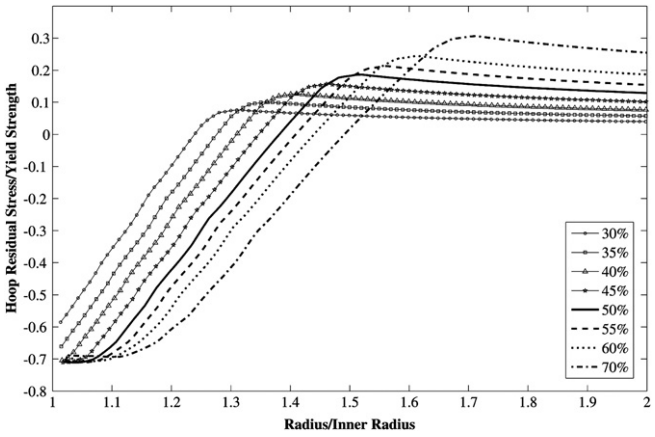

Fig. 9. Hoop residual stress distribution of A723 spherical vessel for different autofrettage percents.

However, their behavior in unloading is strongly nonlinear and a function of plastic strain in loading. Also, pronounced Bauschinger effect causes the compressive yield strength to be much less than the initial tensional yield strength. Comparison of Figs. 1 and 2 shows that the strain hardening after yielding in loading and the level of nonlinearity in unloading are less in A723 steel. The yield strength of A723 and HB7 steels are considered 1130 and 1160 MPa, respectively.

4. Results and discussion

We used the developed VMP model to study the residual stresses in an autofrettaged spherical pressure vessel with radius ratio of 2, outer radius/inner radius = 2, made of A723 and HB7 steels subjected to different autofrettage percents. For this purpose, at first, the vessel was divided to twenty layers with equal thicknesses. Here in the loading session of developed VMP code, materials behavior from loading part of the curves shown in Figs. 1 and 2 was exactly assigned to the all layers and the problem was solved for loading. Once the state of the equivalent stresses of loading was obtained for each layer, the corresponding unloading curve was chosen and assigned by linear interpolation between the unloading curves of Figs. 1 and 2. Finally, residual stress distribution was determined by subtracting loading and unloading stresses of layers.

We compared the results of our analyses with the results obtained from finite element method. A finite element model of the pressure vessel subjected to internal pressure was constructed using commercially available software, ANSYS [24]. The quadratic symmetric 8-node element is employed for the inelastic FE analyses. The boundary condition and mesh distribution of the FE model employed in this study is presented in Fig. 3.

Figs. 4 and 5 show hoop ($\sigma_\theta = \sigma_\varphi$) and radial ($\sigma_r$) residual stresses in an A723 spherical pressure vessel subjected to autofrettage pressure of 1300 MPa, respectively. The results shown are obtained by the following methods:

1. Finite element method using actual material model in loading and isotropic hardening (IH) model in unloading.
2. VMP method using actual material model in loading and isotropic hardening (IH) model in unloading.
3. VMP method using actual material model both in loading and unloading.

Figs. 6 and 7 show similar results for a HB7 spherical pressure vessel which is subjected to 1330 MPa autofrettage pressure. It can be seen that there is a good agreement between finite element and developed VMP results when the material models used are the same. The significant difference between the calculated hoop residual stresses near the inner radius, based on different material models, is evident in Figs. 4 and 6. Here, the errors caused by using isotropic hardening model in analyses of A723 and HB7 vessels are 30.2% and 23.7% at the inner radius of the vessel, respectively. As previously mentioned, the main purpose of the autofrettage process is producing compressive hoop residual stresses near the

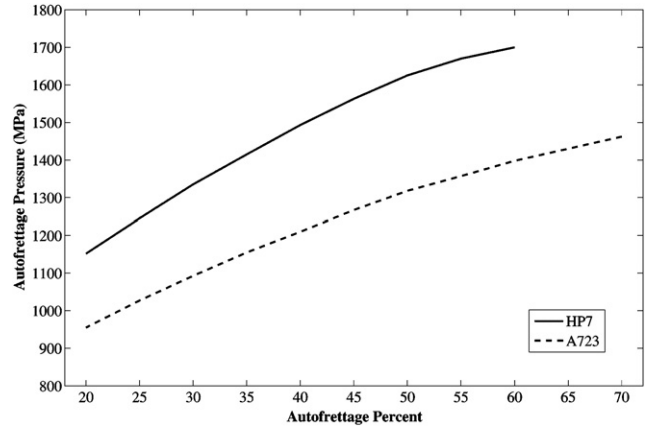

Fig. 8. Required autofrettage pressure for creating different autofrettage percents in A723 and HB7 spherical vessels.

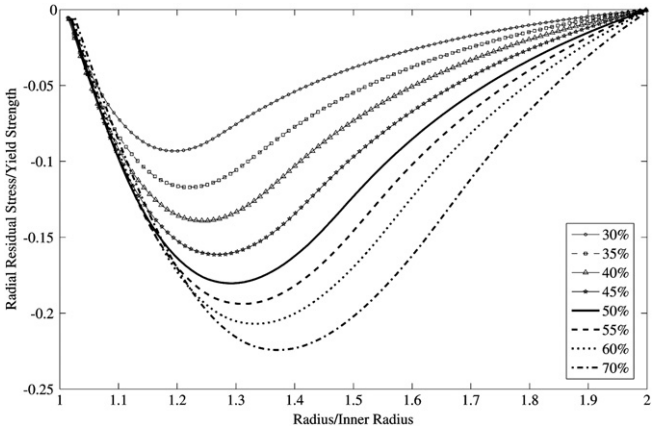

Fig. 10. Radial residual stress distribution of A723 spherical vessel for different autofrettage percents.

inner radius of pressure vessels for increasing their fatigue life. Consequently, the developed errors may lead to the over estimation of fatigue life which demonstrates the importance of using actual material model in analyses. Similar investigations on residual stress analyses (e.g. [25]) reported the existence and increasing trend of the characterized error by increasing autofrettage pressure in cylindrical pressure vessels.

Fig. 8 shows required autofrettage pressure for producing different autofrettage percents in A723 and HB7 spherical vessels, with radius ratio of 2, calculated by VMP method. The autofrettage percent is defined as the ratio of thickness of the vessel undergoing plastic deformation during initial pressurization to the total thickness of the vessel.

Figs. 9 and 10 show hoop and radial residual stresses in an A723 spherical pressure vessel under various autofrettage percents, respectively. These figures show that the creation of tensional hoop residual stress near the outer radius of the vessel is inevitable in all percentages of autofrettage. Although the beneficial effect of the inner compressive hoop residual stress is usually notable, the tensional exterior residual stress, especially in the cases that the vessel is employed in corrosive environment, is unfavorable. Therefore, optimum autofrettage is introduced as a process in which high compressive and low tensional hoop residual stress are simultaneously produced near the inner and outer radii of the vessel respectively. As the Fig. 9 shows, by increasing autofrettage percent from 30% to 70%, the outer tensional hoop residual stress gradually increases. With increasing autofrettage percent from 30% to about 40%, the inner compressive hoop residual stress, $\sigma_{\theta i}^{res}$, also increases. While in the higher percents, $\sigma_{\theta i}^{res}$ remains approximately constant. This phenomenon can be attributed to low strain hardening of A723 steel both in loading and unloading (Fig. 1). Accordingly, about 40% can be recommended as the optimum autofrettage percent for the vessel with the mentioned specifications.

Figs. 11 and 12 show similar results to Figs. 9 and 10, but for a spherical pressure vessel made of HB7 steel. In Fig. 11, it is obvious that outer tensional and inner compressive hoop residual stresses gradually increase by enhancing autofrettage percents from 20% to 70%. The obtained results show the same trend in higher percentages of autofrettage too. Thus, the proposed criterion can not be applicable in the case of HB7 spherical pressure vessel. The observed increasing trend of $\sigma_{\theta i}^{res}$ in the vessel made of HB7 can be connected with high strain hardening of HB7 steel in loading and unloading even at high strains (Fig. 2).

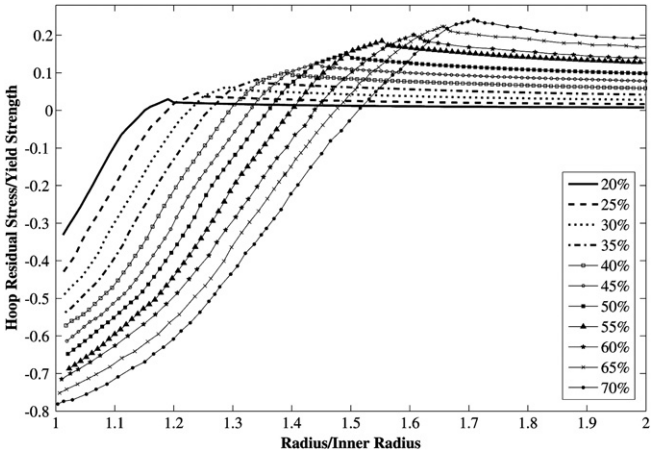

Fig. 11. Hoop residual stress distribution of HB7 spherical vessel for different autofrettage percents.

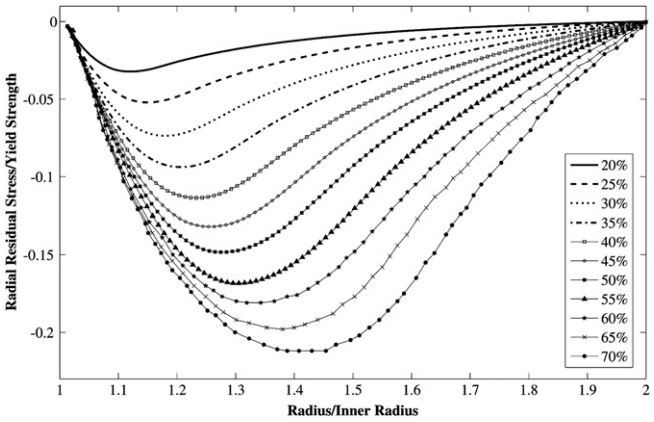

Fig. 12. Radial residual stress distribution of HB7 spherical vessel for different autofrettage percents.

5. Conclusion

The residual stress distribution induced in autofrettaged spherical pressure vessels made of A723 and HB7 steels, based on their actual behavior in loading and unloading was evaluated by developing an extension of the variable material property method. The results showed that the magnitudes of calculated hoop residual stress at the inner radius of the vessel, $\sigma_{\theta i}^{res}$, strongly depend on the employed material model. It was investigated that usage of isotropic hardening model in analysis leads to significant overestimation in $\sigma_{\theta i}^{res}$. The autofrettage percent by which high compressive and relatively low tensional hoop residual stress are simultaneously attainable near the inner and outer radii of the vessel was introduced as the optimum percentage of autofrettage. It was observed that in the case of A723 spherical vessel with radius ratio of 2, by increasing autofrettage percent, the inner compressive hoop residual stress remains constant above a specific autofrettage percent, about 40%, while the outer hoop tensional stress gradually increases. This phenomenon was attributed to low strain hardening of A723 steel in loading and unloading. Consequently, based on the mentioned criterion, the optimum autofrettage percent for an A723 spherical vessel with radius ratio of 2 was calculated about 40%. However, because of high strain hardening of HB7 steel in both loading and unloading even at high strains which cause to increasing trend of hoop residual stress at the inner radius of the vessel, optimum autofrettage percent can not be defined for the HB7 vessel, based on this criterion.

References

[1] Rees DWA. Autofrettage theory and fatigue life of open-ended cylinders. J Strain Anal Eng 1990;25:109–21.
[2] Thumser R, Bergmann JW, Vormwald M. Residual stress fields and fatigue analysis of autofrettaged parts. Int J Press Ves Pip 2002;79:113–7.
[3] Webster GA, Ezeilo AN. Residual stress distributions and their influence on fatigue lifetimes. Int J Fatigue 2001;23:375–83.
[4] Chen PCT. Bauschinger and hardening effect on residual stresses in an autofrettaged thick-walled cylinder. J Press Vess-T ASME 1986;108:108–12.
[5] Majzoobi GH, Farrahi GH, Mahmoudi AH. A finite element simulation and an experimental study of autofrettage for strain hardened thick-walled cylinders. Mat Sci Eng A 2003;359:326–31.
[6] Manning WRD. Bursting pressure as the basis for cylinder design. J Press Vess-T ASME 1978;100:374–81.
[7] Zhu R, Yang J. Autofrettage of thick cylinders. Int J Press Vess Pip 1998;75:443–6.
[8] Adibi-Asl R, Livieri P. Analytical approach in autofrettaged spherical pressure vessels considering the Bauschinger effect. J Press Vess-T 2007;129:411–9.
[9] Darijani H, Kargarnovin MH, Naghdabadi R. Design of spherical vessels under steady-state thermal loading using thermo-elasto-plastic concept. Int J Press Ves Pip 2009;86:143–52.

[10] Kargarnovin MH, Darijani H, Naghdabadi R. Evaluation of the optimum pre-stressing pressure and wall thickness determination of thick-walled spherical vessels under internal pressure. J Frankl Inst 2007;344:439–51.
[11] Kargarnovin MH, Rezai Zarei A, Darijani H. Wall thickness optimization of thick-walled spherical vessel using thermo-elasto-plastic concept. Int J Press Ves Pip 2005;82:379–85.
[12] Parker AP, Huang X. Autofrettage and reautofrettage of a spherical pressure vessel. J Press Vess-T 2007;129:83–8.
[13] Perl M, Perry J. The beneficial contribution of realistic autofrettage to the load-carrying capacity of thick-walled spherical pressure vessels. J Press Vess-T;132:011204–6.
[14] Parker AP, Underwood JH. Influence of the Bauschinger effect on residual stress and fatigue lifetimes in autofrettaged thick-walled cylinders. ASTM Special Technical Publication 1999:565–83.
[15] Parker AP, Underwood JH, Kendall DP. Bauschinger effect design procedures for autofrettaged tubes including material removal and Sachs' method. J Press Vess-T ASME 1999;121:430–7.
[16] Jahed H, Dubey RN. An axisymmetric method of elastic-plastic analysis capable of predicting residual stress field. J Press Vess-T 1997;119: 264–73.
[17] Farrahi GH, Hosseinian E, Assempour A. General variable material property formulation for the solution of autofrettaged thick-walled tubes with constant axial strains. J Press Vess-T 2008;130. 041209–7.
[18] Haghpanah Jahromi B, Farrahi GH, Maleki M, Nayeb-Hashemi H, Vaziri A. Residual stresses in autofrettaged vessel made of functionally graded material. Eng Struct 2009;31:2930–5.
[19] Jahed H, Farshi B, Bidabadi J. Minimum weight design of inhomogeneous rotating discs. Int J Press Ves Pip 2005;82:35–41.
[20] Jahed H, Farshi B, Karimi M. Optimum autofrettage and shrink-Fit combination in multi-layer cylinders. J Press Vess-T 2006;128:196–200.
[21] Jahed H, Shirazi R. Loading and unloading behaviour of a thermoplastic disc. Int J Press Ves Pip 2001;78:637–45.
[22] Troiano E, Parker AP, Underwood JH. Mechanisms and modeling comparing HB7 and A723 high strength pressure vessel steels. J Press Vess-T 2004;126:473–7.
[23] Troiano E, Parker AP, Underwood J, Mossey C. Experimental data, numerical fit and fatigue life calculations relating to the Bauschinger effect in high strength armament steels. J Press Vess-T 2003;125:330–4.
[24] Ansys 8.0, Ansys Inc.
[25] Parker AP. Autofrettage of open-end tubes-pressures, stresses, strains, and code comparisons. J Press Vess-T 2001;123:271–81.